Article:

Wang, Q, Shen, J, Glover, PWJ orcid.org/0000-0003-1715-5474 et al. (2 more authors) (2022) Improving the Prediction of Production Loss in Heterogeneous Tight Gas Reservoirs Using Dynamic Threshold Pressure. Energy and Fuels, 36 (19). pp. 11991-12003. ISSN 0887-0624

https://doi.org/10.1021/acs.energyfuels.2c02713

Improving prediction of production loss in heterogeneous tight gas reservoirs using dynamic threshold pressure

Qian Wang[1*], Jian Shen[1], Paul W.J. Glover[2], Piroska Lorinczi[2], Ian Duncan[3]

1 School of Resources and Geosciences, China University of Mining and Technology, Xuzhou, 221000, China
2 School of Earth and Environment, University of Leeds, Leeds, LS2 9JT, UK
3 Bureau of Economic Geology, The University of Texas at Austin, Austin, Texas 78713
*Corresponding Author, Qian Wang, wqian6200@cumt.edu.cn

Abstract: Tight gas reservoirs commonly exhibit complex pore-throat structures which lead to strong heterogeneity and anisotropy in their permeability tensors. Conventionally, a constant threshold pressure gradient (TPG) has been used to predict the production loss that arises from overcoming the rock's disinclination to flow water and gas through such complex pore-throat structures. The problem is that the TPG is not constant during the production lifetime of a reservoir. In this work we find that using a constant TPG results in large underestimations of gas production. This is because TPG varies significantly with both effective stress and water saturation; an effect which is greater for tight heterogeneous rocks. The sensitivity of TPG to stress and mobile water saturation are themselves controlled by permeability, generating a complex feedback. These dynamic changes in TPG during reservoir production, lead us to rename TPG as the dynamic threshold pressure gradient (DTPG). In the first part of this paper we examine the sensitivity of the DTPG to stress and mobile water saturation for cores with different permeabilities, showing that DTPG increases logarithmically with effective stress, from 0.17 MPa/m to 0.5 MPa/m for a change in effective stress from 0.6 MPa to 30.5 MPa. The DTPG also increases exponentially with mobile water saturation (S_m), being 2.7 to 6.5 times higher at S_m=20% compared to the value at irreducible water saturation. The sensitivity of DTPG to both variables shows a decreasing power law trend with increasing rock permeability. These combined effects generally lead to the DTPG being larger than the conventional TPG. In the second part of this paper we model the effects of using a variable DTPG in place of a constant TPG for the purpose of predicting the production loss associated with the latent pressure barrier in different heterogeneous reservoirs. When the interacting effects of effective stress, water saturation and permeability are taken into account, we find that the threshold pressure is relatively small in heterogeneous reservoirs with a distribution of increasing permeability in the gas flow direction. The constant TPG approach underestimates the production loss by 34-45% with the greatest difference occurring at low gas pressures encountered at the production well, suggesting that gas production wells should be located in areas with high permeability.

Keywords: tight gas reservoirs, permeability heterogeneity, dynamic threshold pressure gradient, stress sensitive, threshold pressure distribution, gas production loss

Introduction

Tight sandstone gas reservoirs have huge gas reserves and very significant potential for development [1-3]. Tight sandstones gas reservoirs have low or ultra-low porosity/permeability, high water saturation, strong heterogeneity, and complex gas-water seepage (flow of gas-water in rock pore-throats) [4-6]. The water film in the complex and fine pore-throats of tight gas reservoir rocks produces greater resistance to seepage [7-10]. The gas in the pore-throats needs to break through, overcoming the capillary resistance to flow from the static state [11]. Consequently, a certain displacement differential pressure is required initially to counteract this resistance, to start and then to maintain the gas flow along the pore-throat path. In tight sandstone gas reservoirs, the threshold pressure gradient (TPG) is both significant and dynamic in the sense that it depends on permeability, effective stress and water saturation [12].

The pore-throat structure of the rock is the key factor controlling TPG in tight sandstone rocks [13]. The permeability of the rock is related to the complexity of the pore-throat structure [14]. Consequently, rock permeability is considered to have a significant effect on the threshold pressure in tight reservoirs [15]. Moreover, the differential pressure for gas production in tight gas reservoirs is large due to their low permeability. The drop in reservoir fluid pressure during development results in changes in the effective stress on the reservoir rock. The large variation in effective stress results in significant changes to the original small-scale pore-throat structure [16]. In addition, water saturation continues to increase during the development process, changing the water distribution in the rock's pore-throats. The variations in rock effective stress and water distribution lead to changes in the threshold pressure gradient, known as the dynamic threshold pressure gradient (DTPG) effect [17-21]. Sensitivity coefficients are used to describe how sensitive the DTPG is to changes in effective stress and mobile water saturation.

The dynamic nature of the TPG makes it difficult to predict the threshold pressure distribution in reservoirs at different reservoir pressures [22]. The determination of the optimal well spacing between injection and production wells lacks a basis for prediction [23]. In addition, the prediction of gas well production is complicated by the DTPG effect. Existing gas well production formulae have been established using the magnitude of the threshold pressure without taking account of its dynamic nature. The TPG is considered to be a fixed value, and this value is measured at a low effective stress [24]. The predicted threshold pressure with distance is linear according to this value, which inevitably leads to an underestimated calculated gas production loss. Consequently, the predicted gas production is overestimated, resulting in actual production deviating from expected development schedule.

The TPG is affected by rock permeability, especially in the case of tight reservoirs with strong permeability heterogeneity. The calculation of threshold pressure distribution and the prediction of gas production are more complicated, as is the effect of DTPG. Consequently, it is important to understand the distribution of DTPG in tight gas reservoirs [25]. Such understanding can facilitate the design of the appropriate development parameters and well pattern layout to reduce the gas production loss caused by DTPG.

The TPG of tight sandstones at different permeabilities and conditions of water saturation have been tested on cores in previous studies [11-13, 22]. Small rock permeability values are considered to be associated with small pore-throat structures. This agrees with the relevant theoretical petrophysics and with results from nanometer scale 3D scanning of shales [26-30]. Pore-throats with small radii produce large capillary resistance. In addition, more fluid flow channels are blocked with the increased water saturation. Consequently, the combination of low permeabilities and high mobile water saturations result in tight reservoirs with large values of TPG [31-32]. The sensitivity of TPG to mobile water saturation has been tested in our previous studies [22], showing that mobile water has a greater effect on TPG than irreducible water [11]. Moreover, the TPG values increase with effective stress [33], which is attributed to increased capillary resistance due to a decrease in pore-throat size [18, 34]. This is analogous to the stress sensitivity of permeability [22].

The sensitivity of DTPG to stress and mobile water is closely related to permeability and its heterogeneity. However, published studies have not taken into account the heterogenous nature of permeability, the sensitivity of DTPG to effective stress and mobile water saturation and the effects of changing permeabilities, despite the distribution of DTP being closely related to permeability heterogeneity as gas production progresses. Calculations based on our experimental tests reported in this work lead us to conclude that, there are large differences in the DTPG distributions in reservoirs with the same average permeability but different heterogeneity distributions under the same stress conditions. Development parameters and well deployment for different permeability heterogeneity distributions in tight reservoirs can then be established to reduce the threshold pressure.

Unfortunately, the distribution of DTPG in tight reservoirs with permeability heterogeneity has not previously been studied. Research on the threshold pressure variation with distance from injection and production wells, and the gas production loss due to DTPG in the permeability-heterogeneous tight reservoir has also not been reported.

In this paper, we study the sensitivity of rock DTPG to effective stress and mobile water saturation in heterogeneous tight gas reservoirs, and ultimately predict the distribution of DTPG within such reservoirs. Measurements of the DTPG of tight sandstone cores with different permeabilities have been carried out by using the improved bubble method [22]. The variation in characteristics of the DTPG at different effective stress values and saturations of mobile water has also been studied. The impact of rock permeability on effective stress sensitivity coefficient and mobile water sensitivity coefficient of DTPG has been analyzed quantitatively. The threshold pressure distribution in the heterogeneous reservoir has then been calculated using the DTPG. In particular, the influence of the distribution of the permeability heterogeneity and reservoir pressures on the threshold pressure distribution are reported, and gas production loss related to these issues is discussed. The results with DTPG were compared with those corresponding to the conventional fixed threshold pressure gradient (FTPG). The results provide both the base data and theoretical basis that support the prediction of threshold pressure in tight gas reservoirs and calculation of gas production in this type of reservoirs.

Methodology

Materials

Nine sandstone cores (numbered Y1-Y6 and C1-C3) were chosen from a target tight reservoir at a depth of 3000-3100 m. The cores C1-C3 were divided into two equal parts, each 3.5 cm long (Table 1). The reservoir temperature is 82±1.8°C, the rock porosity varied from 3% to 13%, with an arithmetic mean of 8.1%, while the permeability varied between 0.02×10^{-3} μm^2 and 0.2×10^{-3} μm^2, with an arithmetic mean of 0.08×10^{-3} μm^2 and a geometric mean of 0.09×10^{-3} μm^2. Cores Y1-Y6 were cut so that all cores were 7 cm in length (Table 1). The samples were studied by X-ray diffraction for elemental and mineral composition. The average total content of quartz and feldspar of these samples is greater than 75%.

The brine used in all experimental tests was prepared to match known formation water data for the field (Table 2). Cores were immersed in brine and aged for 24 hours, to reduce any differences in the wettability of mineral surfaces in different cores as much as possible. This is important in order to reduce the effect of wettability differences on the distribution of gas-water transport through the cores during tests, so that the effect of other parameters can be more easily ascertained [35]. Pure humidified CH_4 were used to represent the gas of reservoir in the experiments.

Table 1. Basic parameters of the core samples.

No.	L (cm)	D (cm)	ϕ(%)	k (10^{-3} μm^2)	S_{wi} (%)
Y1	7.093	2.535	5.35	0.0258	48.5
Y2	7.117	2.527	8.843	0.0346	50.2
Y3	7.081	2.521	7.975	0.0459	45.7
Y4	7.066	2.534	7.737	0.0781	44.8
Y5	7.121	2.532	8.506	0.1158	40.6
Y6	7.216	2.524	9.008	0.1224	38.9
C1-1	3.652	2.521	6.868	0.0251	
C2-1	3.493	2.522	8.102	0.0679	47.9
C3-1	3.817	2.526	9.642	0.1295	
C1-2	3.611	2.521	6.868	0.0248	
C2-2	3.473	2.522	8.102	0.0684	48.5
C3-2	3.784	2.526	9.642	0.1253	

Note. L core length, D core diameter, ϕ porosity, k Klinkenberg permeability, S_{wi} irreducible water saturation

Table 2. Physicochemical properties of the reservoir brine measured at 20°C.

Item	Value
Density (g/cm^3)	1.031
pH	6.74
K^+ (mg/L)	2318
Na^+ (mg/L)	1148
Ca^{2+} (mg/L)	4314
Mg^{2+} (mg/L)	390
Cl^- (mg/L)	22344
HCO_3^-(mg/L)	1148
SO_4^{2-}(mg/L)	1809
TDS (mg/L)	41614

TDS = Total dissolved solids

Threshold pressure test method

The threshold pressure values were measured by an improved bubble method [22]. First, a small displacement differential pressure is applied to the core by injecting CH_4. A thin pipette containing air bubbles in dyed water is connected to the outlet end of the core. The displacement differential pressure is then increased continuously. The gas starts to flow in the core when the differential pressure overcomes the capillary resistance, which causes the bubbles to move. At this point, the differential pressure between the two ends of the core is the minimum threshold pressure for which the two phases of gas-water can flow [36]. The bubbles in the thin pipette are monitored by a camera and a computer. Once any movement of bubbles is detected by the camera and the computer, the computer immediately records the pressure data, improving the accuracy of the measurement. During DTPG tests, the differential pressure is monitored by a dynamic differential pressure gauge. This device can continuously monitor the dynamic change of differential pressure on the order of 10^{-6} MPa while the system working pressure is over 50 MPa.

Test equipment and procedures

The main experimental devices are the core displacement system and the matching nuclear magnetic resonance (NMR) test system, as shown in Figure 1.

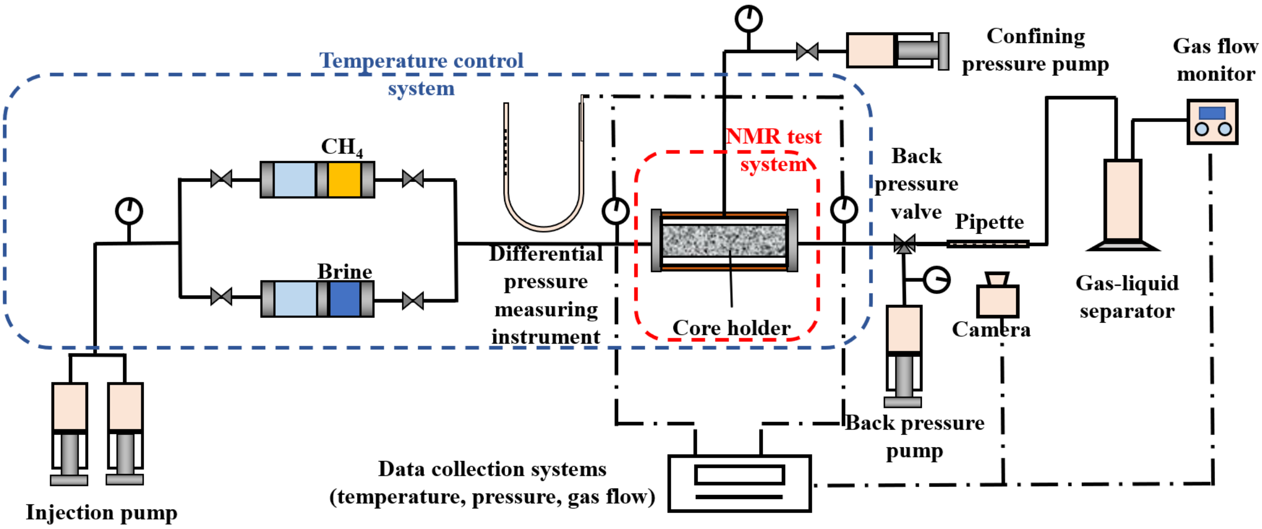

Figure 1. TPG test experimental device.

The measurement steps are as follows,

(1) The fluid transfer vessels were filled with CH_4 and brine together with the core holder were placed in the temperature controlled chamber. The chamber temperature was set to 82°C and left for 24 hours for the temperature to equilibrate in all parts of the heated equipment.

(2) The brine saturated core was placed in the core holder with confining pressure of 31 MPa. The brine in the core was then gradually displaced by CH_4 injection. The core holder was placed in the NMR equipment for NMR scanning. The brine distribution was monitored, and the corresponding brine saturation was calculated. The brine in the core was displaced by CH_4 injection until the water saturation reached specified

pre-defined value.

(3) The pressure at the outlet end of the core was stabilized at 30.4 MPa by the back-pressure pump and the back-pressure valve at irreducible water saturation (S_{wi}). The differential pressure was then increased from a starting value of 1×10^{-3} MPa in increments of 1×10^{-3} MPa by injecting CH_4. At each pressure value, the pressure was stabilized for 3 hours until the bubble movement in the pipette was recognized. The TPG at this back-pressure was recorded. Otherwise, the differential pressure was gradually increased until the bubble moved. The back-pressure was set to the next value in a total of 11 other back-pressure values in the range of 0.5-30.4 MPa, and the TPG values at different pressures were measured, respectively.

(4) Steps (1)-(3) were repeated to test TPG at different mobile water saturations (S_m) at 30.4 MPa back-pressure (in this paper, the irreducible water saturation (S_{wi}) and the water saturation (S_w) of nominally S_{wi}+8%, S_{wi} +15%, and S_{wi} +20%, respectively, in total 4 saturation values, and S_m=S_w- S_{wi}). The core that was in the holder was then replaced, and tests were performed on the other cores.

After the tests, the cores were tested by NMR to measure their water saturation. If the difference in brine saturation was less than 2%, this group experimental data was considered to be reliable. Otherwise, the experimental differential pressure and the TPG value was retested.

Results and discussion

Sensitivity of DTPG to effective stress

The DTPG values of the cores with different effective stresses (P_{eff}) at irreducible water saturation are shown in Figure 2, where the abscissa is logarithmic. The core outlet was connected to the atmosphere in conventional threshold pressure tests. The pressure at the outlet was 0.1 MPa, and the corresponding effective stress was a small fixed value. In fact, the DTPG-P_{eff} curve shows an increasing trend, where the increase is rapid for P_{eff}<5 MPa, with a variation amplitude of 0.1-0.3 MPa/m, and the increase becomes slower for P_{eff}>5 MPa. Consequently, the TPG values tested in conventional threshold pressure tests are relatively small and are also below those encountered during the development of reservoirs.

The total amplitude of the DTPG varies logarithmically between 0.17 and 0.5 MPa/m for variations of P_{eff} between 0.6 and 30.5 MPa. The DTPG-P_{eff} data are well-fitted by a relationship of the following form,

$$\Delta P_{thresh} = \lambda \, ln(P_{eff}) + a \tag{1}$$

where ΔP_{thresh} is TPG (MPa/m), P_{eff} is the effective stress (MPa), and λ and a are fitting coefficients (MPa/m).

The coefficient λ is the slope of the line in Figure 2, a key parameter controlling the increase of the DTPG-P_{eff} curve, called as the DTPG stress sensitivity coefficient. The coefficient λ is used to describe the sensitivity of the DTPG to changes in P_{eff}. The coefficient a determines the average level of the DPTG values, corresponding to the upper ($DPTG_{max}$) and lower ($DPTG_{min}$) limits of DPTG, and λ determines the variation range of DPTG [5].

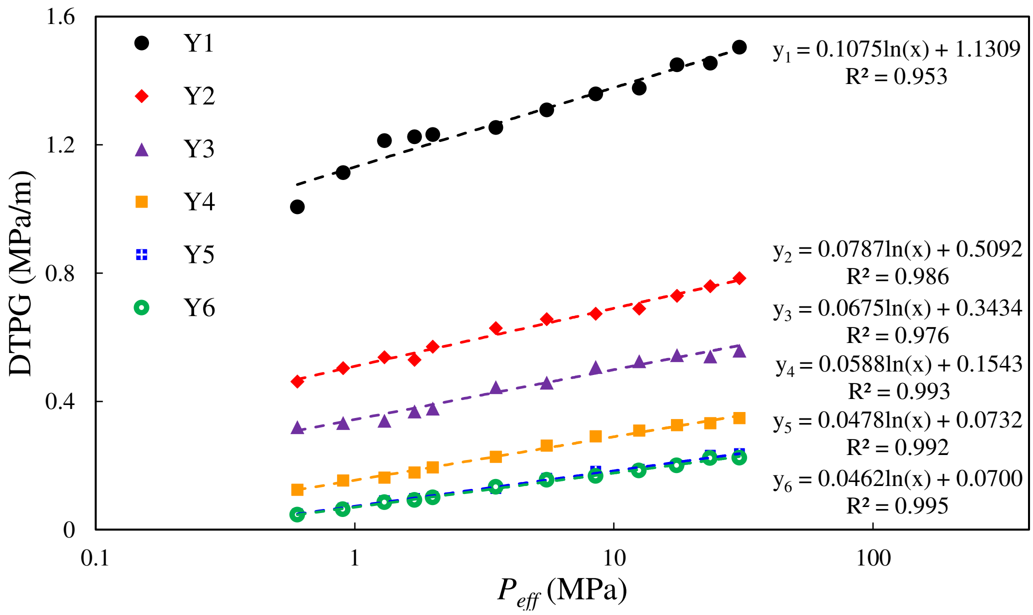

Figure 2. DTPG and effective stress pressure (P_{eff}) of cores at irreducible water saturation (S_{wi}).

The mechanism of rock DPTG stress sensitivity is considered to be similar to that of rock permeability stress sensitivity [37]. The only difference is in the interpretation of the flow process. In the case of permeability, it is assumed that a gas flow is taking place at a given differential gas pressure. Increasing the confining pressure, as shown in Figure 3, reduces the aperture of flow paths, the number of flow paths available for flow, and their connectivity. Closure of flow paths due to increasing overburden pressure reduces all three of these controls on permeability. By contrast DPTG assumes that flow is not taking place and measures the pressure difference required to start flow. Figure 3a shows that for relatively low confining pressures flow is already taking place, indicating that the local DTPG is exceeded in all three channels. As confining pressure increases (Figure 3b), flow is taking place at a differential pressure which is greater than the local DTPG for the top two channels, but has not exceeded the capillary pressure allowing flow in the bottom channel, leaving the channel blocked by a water slug [38]. As overburden pressure increases further (Figure 3c), flow is taking place at a differential pressure which is greater than the local DTPG for only the top channel, while the bottom two channels do not flow because the differential pressure has not exceeded the local DTPG for these channels. Consequently, the control of channel aperture imposed by the overburden pressure controls both the DTPG and the fluid permeability [39].

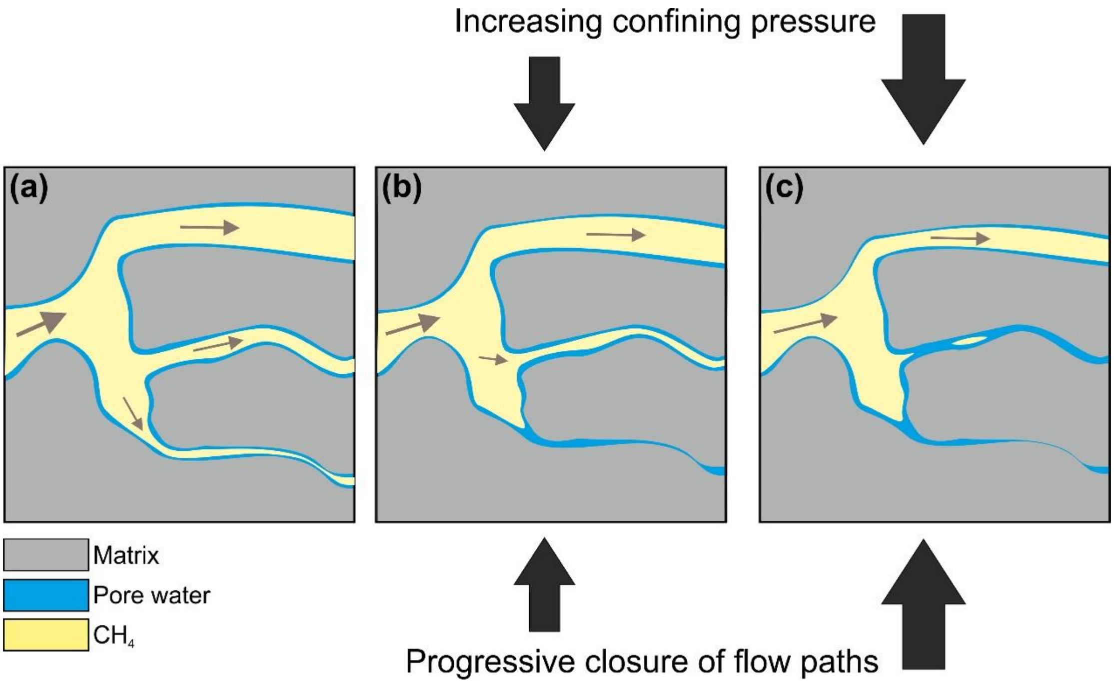

Figure 3. Schematic diagram of the mechanism of DPTG stress sensitivity and permeability stress sensitivity.

We define $DTPG_{min}$ as the DTPG value at minimum effective stress of the rock, and $DTPG_{max}$ as the DTPG value at the maximum effective stress of the rock, as well as the difference between the two, $\Delta DTPG = DTPG_{max} - DTPG_{min}$. Figure 4 shows that all three of these parameters decrease non-linearly as permeability increases. The average pore-throat radius is small in low permeability rock, the capillary resistance formed by the water slug is large, and the TPG value is large. The rate of decrease of the DTPG values with increasing permeability is greater for rocks with smaller permeabilities. This is because the complexity of the pore-throat structure increases exponentially with the decrease of the permeability value at smaller permeability values [40]. The TPG is more sensitive to the variation of the permeability value in lower permeability rocks. The variation range of ΔDTPG also decreases with increasing permeability, indicating that changes in DTPG with effective stress become much smaller as permeability increases.

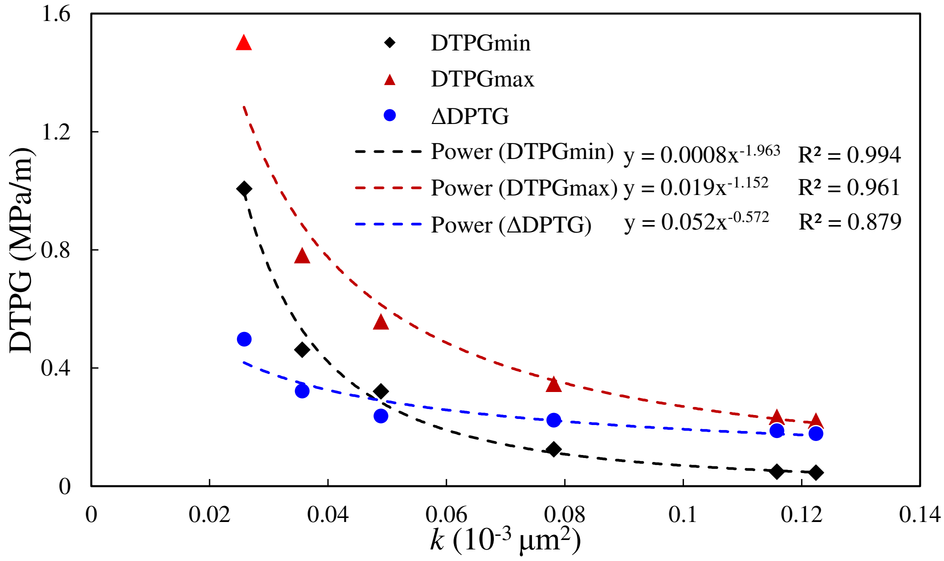

Figure 4. The variations of $DTPG_{max}$ and $DTPG_{min}$ versus core permeability (k). ($DTPG_{max}$, DTPG value at minimum effective stress of rock; $DTPG_{min}$, DTPG value at maximum effective stress of rock; $\Delta DTPG = DTPG_{max} - DTPG_{min}$.)

There are differences in the trend of DTPG-P_{eff} for cores with different permeability, as shown in Figure 2. Large permeabilities correspond to small DTPG values, and the slope of the DTPG-log(P_{eff}) curve is smaller at higher permeabilities, implying that rocks with larger permeabilities exhibit weaker dependence on effective stress.

The λ-k and a-k curves are shown in Figure 5. Both the λ-k curve and a-k curve show downward trends. Smaller permeability samples exhibit larger λ and a coefficients, implying that small permeability samples have both large DTPG values and larger sensitivity to changing effective stress. In particular, λ and a are more sensitive to permeability variations at low permeabilities ($<0.06\times10^{-3}$ μm^2). This is similar to the sensitivity of DTPG to effective stress, because rocks with low permeability have small pore-throats and complex pore-throat structures. A small effective stress variation causes a large change in pore-throat structure and also results in a large change in the water distribution [41]. In this case, the DTPG shows a strong sensitivity to the effective stress.

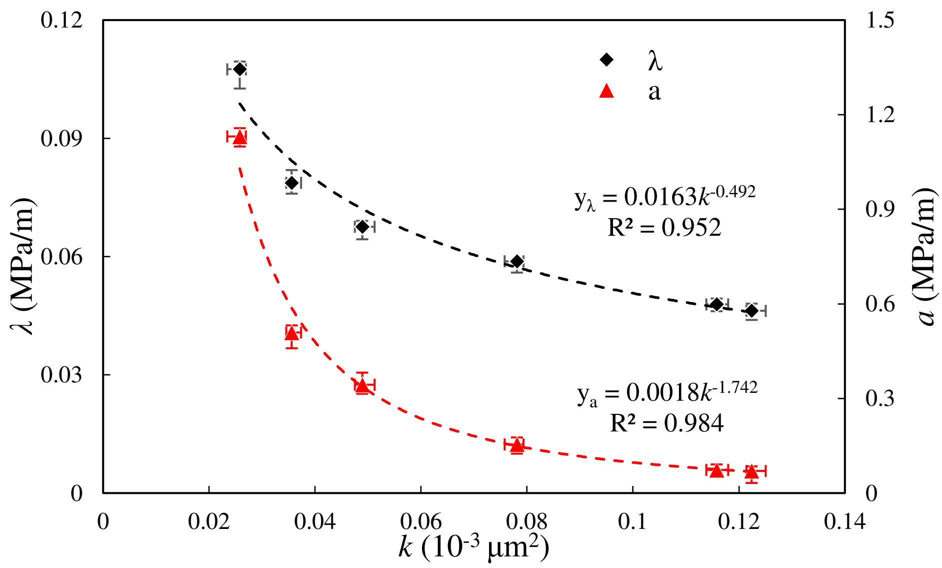

Figure 5. Rock DTPG stress sensitivity coefficient (λ, a) versus core permeability (k).

Sensitivity of DTPG to mobile water

Tight gas reservoirs always have high-water saturations due to the small and complex pore-throat structure [3-4], which results in relatively large values of threshold pressure. Moreover, the water saturation continues to rise during production, which leads directly to a large variation in the water distribution in the pore-throats of the rock [42]. If we consider the scenario illustrated by Figure 3 and then imagine that the water saturation increases, the result will be that there is no change to the pathways that are already blocked, but some of the open pathways may also become blocked by a water slug. The middle channel in Figure 3b is at particular risk of this happening if the local water saturation increases. While this scenario is valid for all overburden pressures, it is more likely to pose a threat at higher overburden pressures where many of the pathways for flow are already small if not already blocked and the DTPG is already high. Consequently, water saturation is also a key factor controlling the DTPG values.

The relationship between the mobile water saturation (S_m) and DTPG at P_{eff} of 0.6 MPa is shown in Figure 6. The DTPG of the cores are 2.7 to 6.5 times the initial value from S_{wi} to an S_m of 25%. The DTPG-S_m relationship shows an exponential increase, exemplified by linear behavior when plotted on semi-logarithmic axes, as here. The relationship is given by,

$$\Delta P_{thresh} = be^{\eta S_m} \tag{2}$$

where ΔP_{thresh} is the TPG (MPa/m), S_m is the mobile water saturation (%), and η (in units of %$^{-1}$) and b

(MPa/m) are fitting coefficients.

The coefficient η is the slope of the line, a key parameter controlling the increase of the value of DTPG with water saturation. This parameter is defined as the DTPG mobile water sensitivity coefficient [22]. The coefficient η is used to describe the sensitivity of the DTPG to changes in saturation of mobile water. The parameter η determines how quickly the curve increases, and the coefficient b is the DTPG value at S_{wi}.

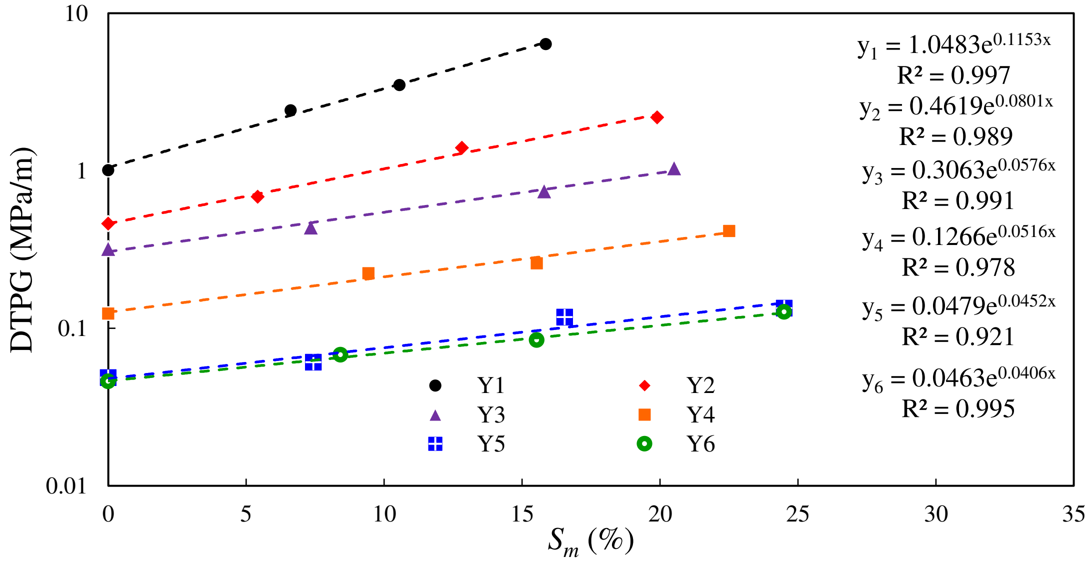

Figure 6. DTPG and mobile water saturation (S_m) of cores at 0.6 MPa effective stress pressure (P_{eff}).

Water is the wetting phase in the rock pores. The irreducible water generally covers the pore walls in the form of water film or fills the smallest pore throats. Gas is the non-wetting phase and is distributed in the center of the relatively larger pore-throats in the flow channel. Water slugs cause relatively little blockage of such larger pore-throat diameter gas flow paths. Contemporaneously, there is free-flowing mobile water in pore-throats at higher saturations than S_{wi}. The thickness of the water film on the pore wall increases as water saturation increases. The mobile water fills the pore-throats that were not originally occupied by the irreducible water, resulting in blockage of the gas transport path for a large range of pore-throat diameters, and the DTPG consequently increases. As S_m continues to increase, some of the relatively larger pore-throats become filled with water [43], extending the range of pore-throat sizes occupied by water slugs to encompass larger pore-throats as well as the smaller pore-throats which were previously not occupied by water slugs. Hence, the total length of flow channel occupied by water slugs increases, which leads to a significantly increase of DTPG. Consequently, the DTPG increases exponentially with S_m.

Compared with the logarithmic increasing trend of DTPG-P_{eff}, the exponential increasing trend of DTPG as a function of S_m indicates that the sensitivity of DTPG to mobile water is stronger than that of effective stress. The increase in water saturation is the direct cause of the existence of the water slug in the pore-throats, which directly produces the gas-water two-phase fluid transport resistance. By contrast, increases in effective stress mainly affects the DTPG by reducing the pore-throat radius when the pores contain water, and plays a more indirect role. The DTPG effect caused by the direct variation of water distribution is consequently more significant than the indirect effect of the pore-throat size change caused by stress sensitivity.

When the water saturation of cores with different permeability increases by the same value, the distribution of the increased mobile water in the pore-throat of different cores is different due to the difference in the complexity of the pore-throat structure, resulting in different impact on the DTPG. The pore-throat radius of low permeability cores is smaller and more complex than that of rocks with higher permeabilities. The increasing mobile water saturation immediately produces a significant increase in the DTPG in low permeability rocks. The overall DTPG-S_m trend is steep and the sensitivity of DPTG to mobile water is affected by rock permeability. The η-k curve is shown in Figure 7. The η-k curve also shows a decreasing power law relationship. The sensitivity coefficient η decreases rapidly with the permeability at low permeability values, while the variation of k has relatively little effect on η at large permeability values. That is, when the permeability is small, the sensitivity of η to k is strong, and when the permeability is large the sensitivity of η to k is weak.

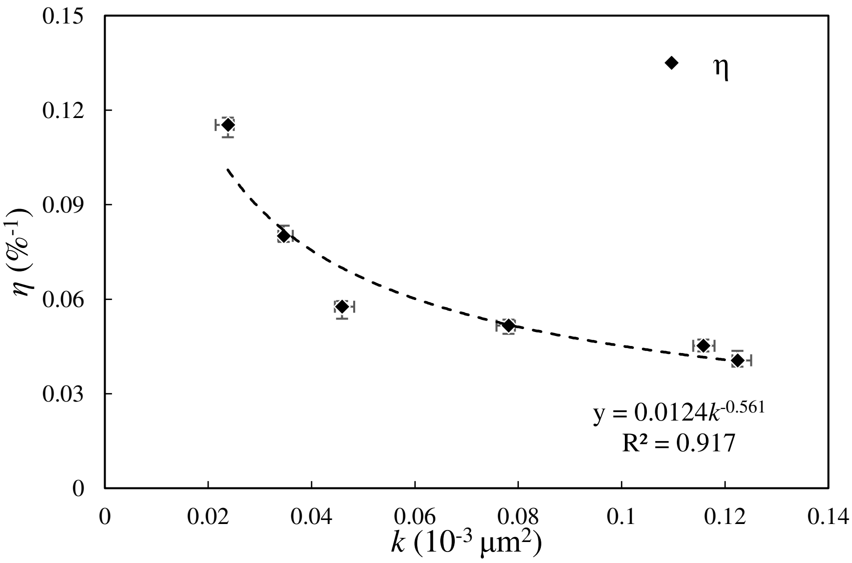

Figure 7. Rock DTPG mobile water sensitivity coefficient (η) versus core permeability (k).

DTPG and permeability heterogeneity

Strong heterogeneity is another major feature of tight gas reservoirs [44]. Cores with different permeability have different pore-throat structures and differences in the water distribution in pore-throats [45]. The heterogeneity resulting from the deliberate combination of short cores to form composite cores with different permeability also affects the DTPG. The effect of heterogeneity on DTPG and its controlling influences has been studied by carrying out measurements on composite cores that are composed of three short cores with different properties. The composite core H1 is composed of short cores C1-1, C2-1, C3-1, with permeability decreasing progressively in the flow direction. The composite core H2 is composed of short cores C1-2, C2-2, C3-2, and has progressively increasing permeability in the flow direction (see Table 1). Figure 8 shows the DTPG-P_{eff} relationships for the composite cores H1 and H2 at different water saturation conditions.

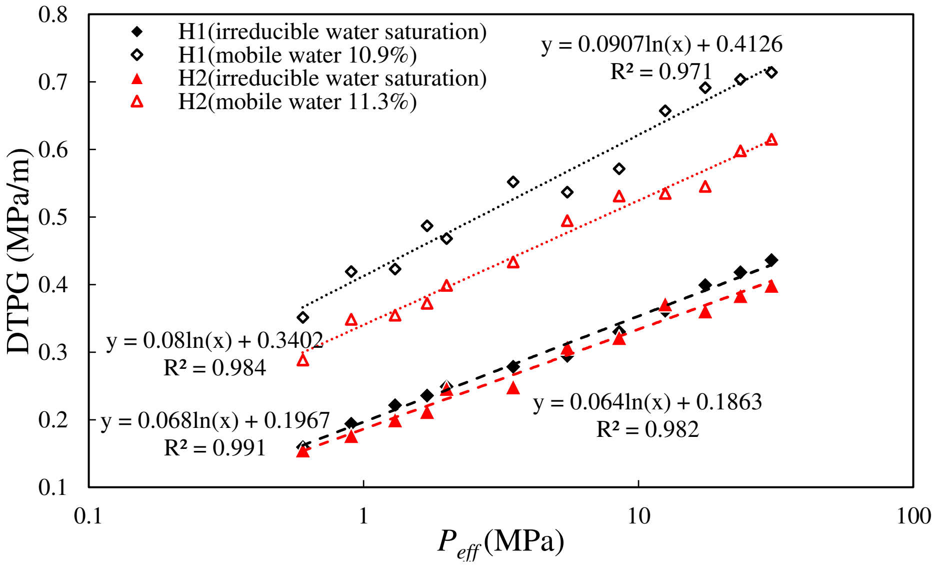

Figure 8. DTPG versus effective stress (P_{eff}) of composite cores.

Similarly to the previously tested cores (Figure 2), the DTPG-P_{eff} curves of both composite cores H1 and H2 also show a logarithmic increasing trend. Moreover, the DTPG-P_{eff} curves of cores H1 and H2 show a large difference at about 11% S_m. That is, the DTPG values and the effective stress sensitivity are different under different fluid flow directions in the heterogeneous core. Clearly, H1 has higher DTPG values and is more sensitive to changes in effective stress. This may be due to the difference in the distribution of mobile water in cores.

Figure 9 shows the NMR T_2 distributions before and after the DTPG tests for the inlet and outlet cores for each composite arrangement. The inlet of core H1 is C3-1 (high permeability core), and the outlet is C1-1 (low permeability core). The inlet end of core H2 is C1-2 (low permeability core), and the outlet is C3-2 (high permeability core). The purpose of this figure is to ascertain what the effect of carrying out the gas-flooding tests are, and whether the change in water saturation and mobility is affected by the permeability and/or position of the core in the composite in order to determine whether the mobility of the water depends on the permeability heterogeneity of the composite cores.

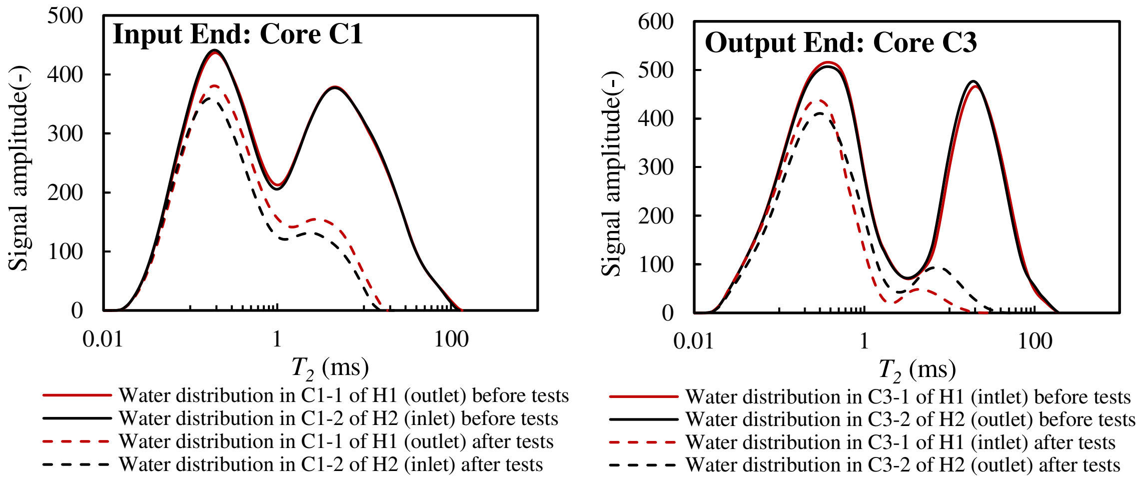

Figure 9. The water distribution in the inlet and outlet of the cores H1 and H2 before and after DTPG tests.

The T_2 distributions in all four of the initially saturated cores (i.e., before the DTPG tests) are bimodal, indicating that (i) the cores have been chosen well to have very similar microstructural characteristics despite having different permeabilities, and (ii) the cores contain both capillary-bound water, represented by the peaks draped around 0.2-0.4 ms, and mobile water, represented by the peaks centered around higher values of T_2. It should be noted that none of the samples conform to the standard, and often erroneous 33 ms cut-off that is often applied blindly in the oil and gas industry. The NMR T_2 distributions measured after the DTPG tests in each case show that most of the mobile water gas been produced from the cores, together with a significant amount of capillary bound water. Water production is marginally greater for cores placed at the outlet.

In the core H1, the permeability decreases along the direction of the displacement differential pressure, and more mobile water is distributed in the small permeability core near the outlet [46]. The DTPG values are larger for cores with smaller permeabilities, as is their sensitivity to changes in effective stress and mobile water as shown in Figure 5 and Figure 7. In the core H2, more mobile water is distributed in the large permeability core near the outlet, the value of DTPG is small and the sensitivity is weak. At irreducible water saturation, the water distribution in cores with different permeability is relatively more uniform. There is a difference in DTPG between H1and H2 at irreducible water saturation, but the difference is small. That difference becomes more significant as water saturation increases. Consequently, the direction of reservoir flow is important from the point of view of DTPG as well as the more conventional considerations of permeability and breakthrough. Hence, the choice of the relative location of injection and production wells can effectively reduce the TPG during the development of heterogeneous tight gas reservoirs.

Threshold pressure distribution

The core test results represent the parameters of a point in the reservoir. The test results cannot characterize the distribution of the TPG in a heterogeneous reservoir at the reservoir scale. Figure 10 shows a schematic diagram of a one-dimensional heterogeneous tight gas reservoir with a length of 50 m at irreducible water saturation. The overburden pressure (P_o) is 31 MPa, and there are two possible permeability distributions, (i) K_1, where the permeability of the reservoir decreases gradually from left to right (0.12×10^{-3} μm^2 to 0.02×10^{-3} μm^2), and (ii) K_2, where the reservoir permeability increases gradually from left to right (0.02×10^{-3} μm^2 to 0.12×10^{-3} μm^2).

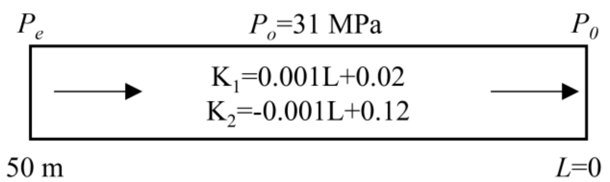

Figure 10. Schematic of one-dimensional linear reservoir with permeability heterogeneity.
The black arrow represents the flow direction, L=0 m represents the production end, P_0 is the pressure at production end, L=50 m represents the reservoir edge, P_e is the pressure at reservoir edge, P_o is the overburden pressure, K_1 represents a decreasing permeability distribution mode along the flow direction, and K_2 represents an increasing permeability distribution mode along the flow direction.

When the differential pressure gradient is larger than the TPG in the reservoir, then the fluid starts to flow [22], that is,

$$\begin{cases} v = 0 & \dfrac{dP}{dL} \le \Delta P_{thresh} \\ v = \dfrac{k_g}{\mu}\left(\dfrac{dP}{dL} - \Delta P_{thresh}\right) & \dfrac{dP}{dL} > \Delta P_{thresh} \end{cases} \tag{3}$$

where v is gas flow rate (m/s), dP/dL is the displacement pressure gradient (MPa/m), P is the pore fluid pressure at any point in the reservoir (MPa), L is the distance from the production well (m), ΔP_{thresh} is the TPG (MPa/m), k_g is the gas permeability (10^{-3} μm^2), and μ is the gas viscosity (mPa·s).

The conventional TPG is considered to have a fixed value, the threshold pressure increases linearly in the reservoir with the distance (L), and the slope of the straight line is the fixed threshold pressure gradient (FTPG). According to the test results in this paper, the TPG in the reservoir is not a fixed value during the production process. It is expected that the relationship between the threshold pressure and distance is not linear. Moreover, the required cumulative displacement differential pressure increases to overcome the threshold pressure. The corresponding P at any position in reservoir also increases when the pressure at the production end is set at a higher value, while the P_{eff} decreases, the DTPG decreases. When the P_e is increased continuously to overcome the threshold pressure, the threshold pressure decreases. The value of P_e and threshold pressure are coupled with each other and change dynamically [22].

In the one-dimensional heterogeneous tight gas reservoir, when the value of the pressure P_0 at L=0 m is determined (which can be considered as the pressure at the production well), there is a minimum P_e value (P_{emin}) at the reservoir edge (L=50 m), which is just large enough for the gas to start flowing. Hence, the value of P_{emin} is the minimum pressure when gas starts flowing. The threshold pressure of the gas-water two-phase transport at P_{emin} in reservoirs is the maximum, which is P_{emin} -P_0. The displacement pressure gradient is just larger than the DTPG at any position in reservoir [11].

$$\frac{dP}{dL} = \Delta P_{thresh} \tag{4}$$

According to the test results of DTPG stress sensitivity at irreducible water saturation of tight gas reservoir rock that we have reported previously in this paper, the DTPG in the reservoir is,

$$\begin{cases} \Delta P_{thresh} = \lambda\, ln\left(P_{eff}\right) + a \\ \lambda = 0.0163k^{-0.492} \\ a = 0.0018\ \ k^{-1.742} \end{cases}$$

$$
\begin{aligned}
k_1 &= 0.001L + 0.02 \\
k_2 &= -0.001L + 0.12 \\
P_{eff} &= P_o - P
\end{aligned}
\tag{5}
$$

Combining Eqs. (4) and (5), the iterative trial calculation can be performed by using MATLAB tools, and the algorithm is shown in Figure 11. In this paper we set the initial value P_0 to three values, 1, 5, and 15 MPa.

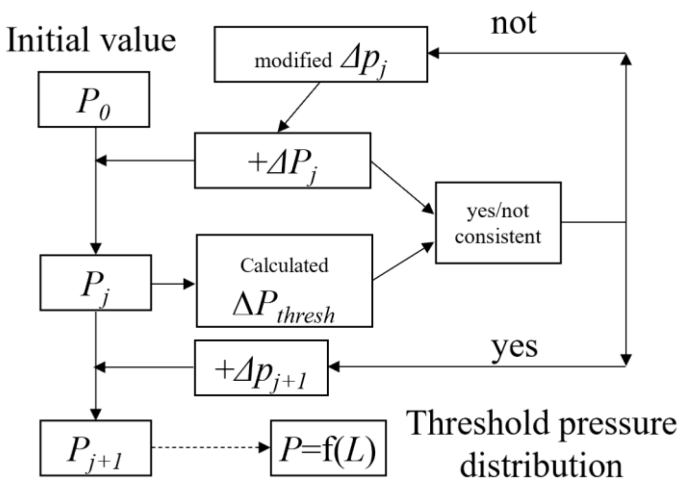

Figure 11. Schematic of method for calculating the threshold pressure distribution in one-dimensional linear reservoir with permeability heterogeneity.

The calculated results of threshold pressure are compared with the results for a FTPG in Figure 12. The effect of effective stress is not considered in the conventional TPG tests, the effective stress of the rock during the tests is small. Consequently, the FTPG is taken as the value of $DTPG_{min}$ (k) in Figure 4, and the FTPG is only related to the permeability of rock [16,47]. The distribution of fixed threshold pressure (FTP) was calculated based on $DTPG_{min}$ (k).

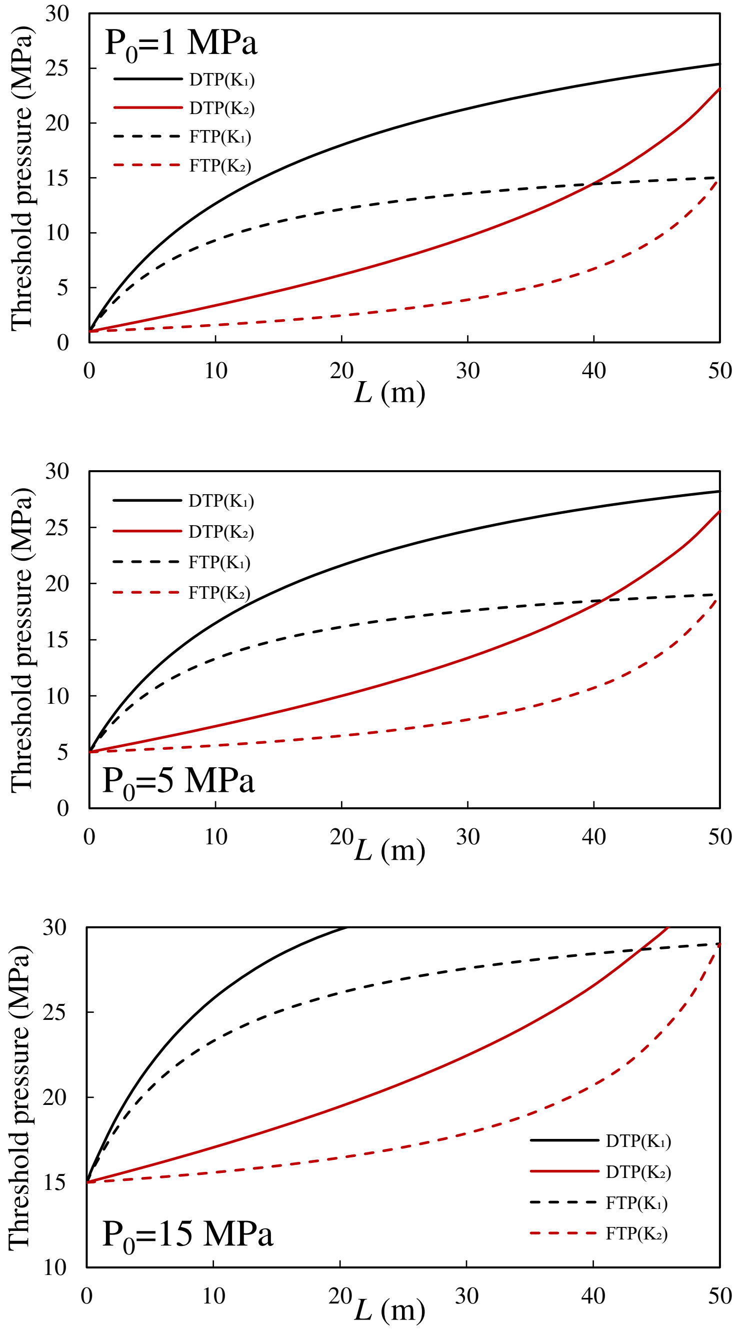

Figure 12. Threshold pressure distribution with length (L) in heterogeneous reservoirs.
DTP is threshold pressure corresponding to the DTPG, FTP is the threshold pressure corresponding to the FTPG. K_1 represents a decreasing permeability along the flow direction, K_2 represents an increasing permeability along the flow direction. (The value of DTP+15MPa is over the overburden pressure 31MPa when L>20 m for K_1 and L>46 m for K_2, the 15 MPa curves of DTP are short.)

As shown in Figure 12, the FTP of the permeability distribution K_1 increases rapidly with L, and then increases slowly. The FTP of the permeability distribution K_2 first increases slowly with L, and then increases rapidly towards the production end. The shape of the FTP-L curves is the same at different mean pore fluid pressures. The total threshold pressure that needs to be overcome to start the flow of gas-water in the reservoir is the same, which is 15 MPa (P_e-P_0), regardless of the value of P_0. The shape of DTP-L curve is similar to that of the FTP-L curve, while the values of DTP are larger than FTP.

Figure 13 shows the relationship between the DTPG and FTPG and the permeability at P_0=1 MPa and at P_{emin} for the permeability distributions K_1 and K_2. The TPG values of rocks with the same permeability are different for the two different permeability distributions, K_1 and K_2. This is because the effective stress varies according to location differently for the two permeability distributions, irrespective of the rock having the same mean permeability. This results in the different values of P_{emin} in the reservoirs with different heterogeneity.

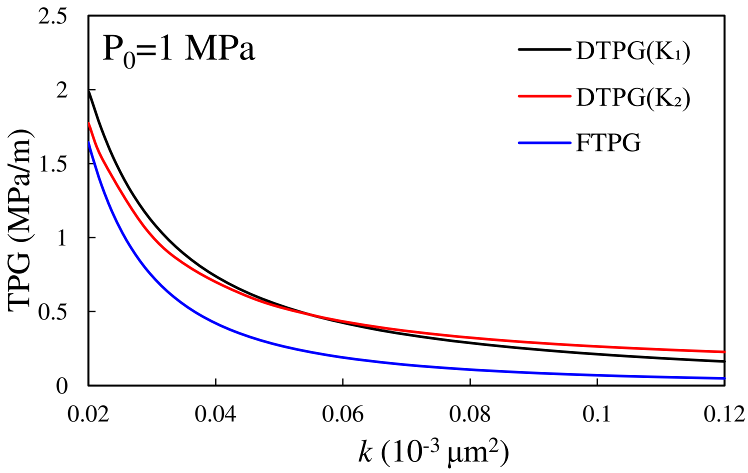

Figure 13. Threshold pressure gradient (TPG) with rock permeability (k) in the permeability distribution mode K_1 and K_2 at P_0=1 MPa and at P_{emin}.

In particular, P_{emin} of permeability distribution K_1 is greater than that of permeability distribution K_2 (Figure 12). The P_{emin} of K_1 are 2.2 MPa larger than that of K_2 at P_0=1, and 1.8 MPa at P_0=5 MPa, respectively. This is because the pore fluid pressure (P) value is small at the production end, the corresponding P_{eff} value is large, and the P_{eff} value is the largest at L=0 m. Consequently, the rock DTPG sensitivity at the production end is affected by a large stress. In the case of permeability distribution mode K_1, the DTPG values are large and the DTPG stress sensitivity is strong at the production end due to the small rock permeability. In the case of permeability distribution mode K_2, the rock permeability at the production end is large. The DTPG has a relatively weak sensitivity to stress at the production end, these rocks have a relatively small DTPG values. The overall result is that the total threshold pressure for 50 m reservoir of permeability distribution K_1 is greater than that of K_2. Furthermore, this difference in threshold pressure between K_1 and K_2 is smaller at high reservoir pressures. This is due to the weak stress sensitivity of rock DTPG at high pore fluid pressures.

Consequently, the production well should be set at the position with high permeability. The gas flows from the position with low permeability to the position with high permeability, to reduce the overall threshold pressure. The differences in permeability distributions have less effect on the resulting total threshold pressure at higher pressures than that at lower pressures. However, when P_0 is higher than a certain value (for example, P_0=15 MPa), the total threshold pressure value in the K_1 permeability distribution is larger than the maximum displacement differential pressure (P_e<31 MPa) at a small L value. The gas in the reservoir at L>20 m cannot start to flow. In the case of K_2 distribution mode, threshold pressure is smaller than maximum displacement differential pressure at L<46 m. The gas production area is larger in reservoirs with K_2-type permeability distribution. More specific data of difference in threshold pressure between K_1 and K_2 distributions (ΔDTP-L curve) is shown in Figure 14.

Interestingly, the inference made above that the production well should be set at the position with high permeability, is the same inference that has been arrived at using Advanced Fractal Reservoir Modelling (AFRM) of heterogeneous and anisotropic reservoirs [48-49]. In this research production optimization was tested for well placement randomly, and for all combinations of injection and production wells deliberately placed in fractally-distributed range of permeabilities from low to high permeability [50]. The results showed that best production occurred when both injection and production wells were deliberately placed in high permeability rocks [51].

The ΔDTP-L curve showed a trend of rapid increase at first and then a rapid decrease. The K_1 permeability distribution mode is unfavorable for gas flow, especially at a high P_0 (for example, P_0=15 MPa). Because the value of total threshold pressure reaches the maximum differential pressure within a short distance from the production end. The gas cannot start to flow without additional fluid injection (such as CO_2 injection). On the other hand, a large P_0 means a small value of the whole effective stress of the reservoir rock, and a small ΔDTP value. Consequently, the selection of the production end P_0 cannot be too large or too small, and there is a moderate value.

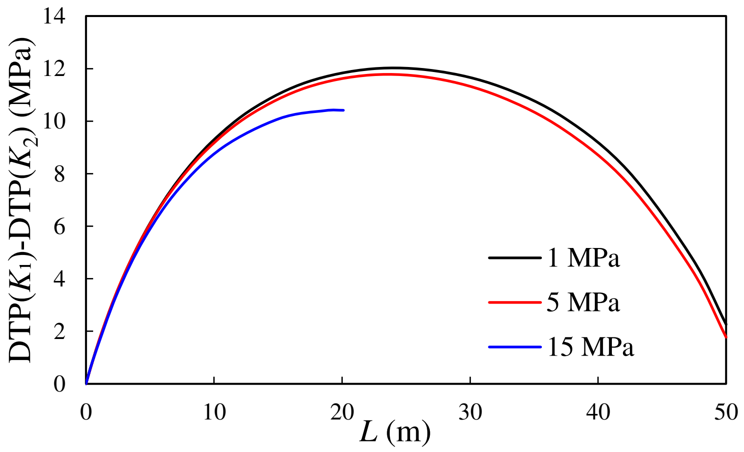

Figure 14. Difference in dynamic threshold pressure (DTP) distribution between K_1 and K_2 with length at different values of P_0.

The difference between DTP and FTP in case of distribution K_1 is shown in Figure 15. This difference increases with L, and the difference becomes smaller at higher P_0. It shows that when the TPG is considered to be a fixed value, a large well spacing results in a large prediction error of threshold pressure, and the error is smaller at higher pressures.

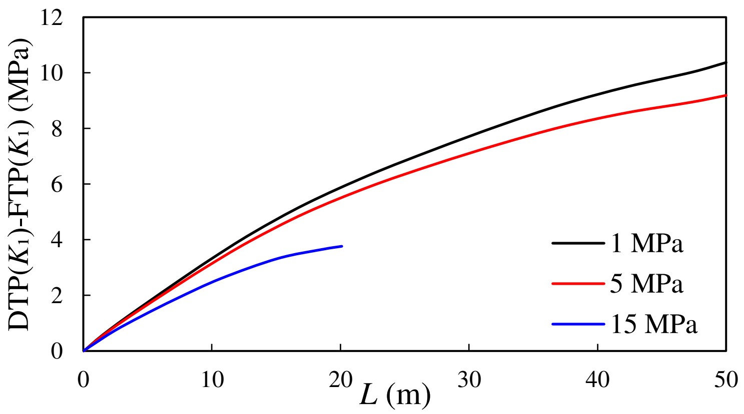

Figure 15. Difference between dynamic threshold pressure (DTP) distribution and fixed threshold pressure (FTP) distribution with length (L) in K_1 distribution at different values of P_0.

Gas production loss

The TPG needs to be overcome before production can start, and in a sense, it consumes a certain displacement differential pressure, resulting in a part of gas production loss of the reservoir. As we have seen, there are differences in the distribution of FTPG and DTPG in heterogeneous reservoirs. Traditionally, the prediction of gas well production loss based on a FTPG value inevitably leads to deviations from expected production values. The results exhibited previously in this paper indicate that the predicted value of the production loss has conventionally been underestimated.

In order to explore the impact of DTPG and reservoir permeability heterogeneity on gas production capacity loss in heterogeneous reservoirs, a cylindrical coordinate, horizontal and equal-thickness heterogeneity model has been established. Once again, we have explored the results from two permeability distributions, K_1 and K_2. The production well is in the centre of the model, as shown in Figure 16.

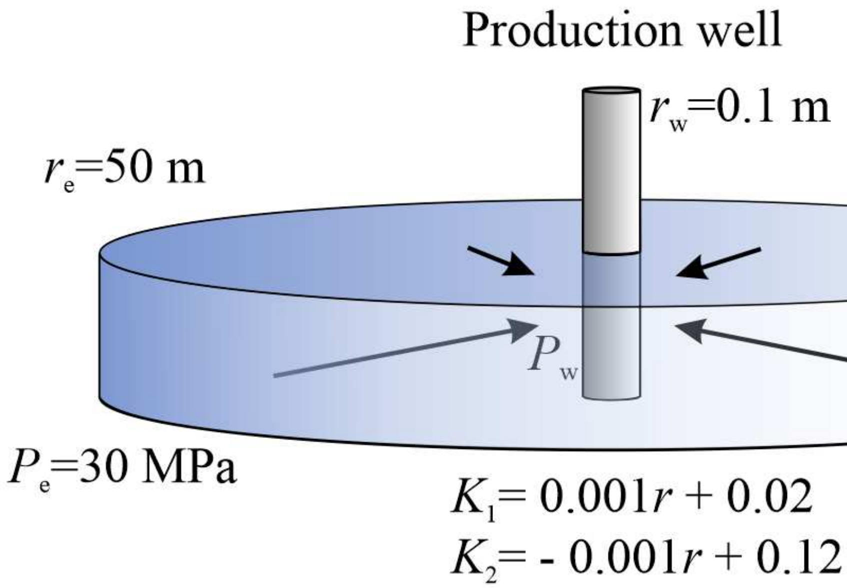

Figure 16. Schematic diagram of a heterogeneous reservoir. The black arrows represent the flow direction, r_e is the radius of the model, P_e is the pressure at the edge of the reservoir, r_w is the radius of the gas production well, P_w is the bottom hole flowing pressure, K_1 represents a decreasing permeability distribution towards the production well, and K_2 represents an increasing permeability distribution towards the production well.

The gas flow at radius r in the reservoir is [52],

$$\begin{cases} q_0 = \frac{2\pi rhK_g}{\mu}\frac{dp}{dr} & \text{(Without TPG)} \\ q_1 = \frac{2\pi rhK_g}{\mu}\left(\frac{dp}{dr} - \Delta P_{thresh-F}\right) & \text{(FTPG)} \\ q_2 = \frac{2\pi rhK_g}{\mu}\left(\frac{dp}{dr} - \Delta P_{thresh-K_1}(P)\right) & \text{(DTPG-}K_1\text{)} \\ q_3 = \frac{2\pi rhK_g}{\mu}\left(\frac{dp}{dr} - \Delta P_{thresh-K_2}(P)\right) & \text{(DTPG-}K_2\text{)} \end{cases}$$

(6)

The gas well production Q_0 without TPG is used as the benchmark, the gas well production loss caused by TPG is,

$$L_p(\%) = (100 - \frac{Q}{Q_0} \times 100) \tag{7}$$

where q_0, q_1, q_2, q_3 are the gas flows for each scenario (m^3/s), h is the reservoir thickness (m), L_p is the gas well production loss ratio (%), and Q is the gas well production (m^3/d).

We combine Eqs. (6) and (7) to calculate L_p of gas well at different P_w using MATLAB tool integration, the result is shown in Figure 17.

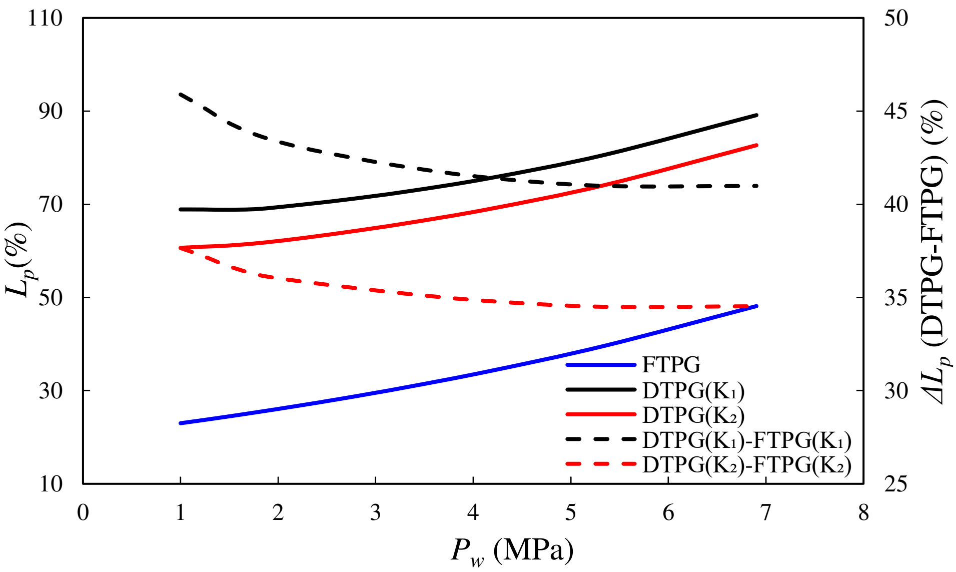

Figure 16. The gas production loss (L_p) due to DTPG and FTPG at different P_w in a heterogeneous reservoir. DTPG is dynamic threshold pressure gradient, FTPG is fixed threshold pressure gradient, and ΔL_p=L_p of DTPG – L_p of FTPG.)

As expected, as shown in Figure 17, the L_p of DTPG is much higher than that of FTPG, because the value of DTPG is higher than that of FTPG. The difference in L_p (ΔL_p) between DTPG and FTPG is 40-45% at P_w of 1 to 7 MPa in the permeability distribution K_1, and ΔL_p is 34-37% in permeability distribution K_2. The value of ΔL_p gradually decreases as P_w increases, but tends to a constant value at high values of P_w. If the TPG is considered to be fixed, large prediction errors of gas well production results, especially at lower P_w. Moreover, L_p increases with P_w, this is due to the fact that a large P_w means a small displacement differential pressure (P_e-P_w). The threshold pressure as the loss of displacement differential pressure accounts for a large proportion of the total displacement differential pressure [22]. The L_p of FTPG is 23-48%, that is, over 20% even at the minimum P_w. The threshold pressure has a greater impact on gas well production in tight gas reservoirs. When the production differential pressure is small, the threshold pressure makes more gas reserves unproducible from the reservoir. The effective development of gas cannot be maintained only by relying on the initial pressure of the reservoir.

Furthermore, the increase trend of L_p-P_w is slow first and then fast in Figure 16. On the one hand, a high P_w results in a small DTPG. On the other hand, a high P_w results in a large L_p. This L_p-P_w behavior is controlled by two opposing factors. It is worth noting that, the value of L_p in the permeability distribution K_1 is higher than that in the permeability distribution K_2. It demonstrates that the permeability distribution mode K_1 is unfavorable for the development of tight gas reservoir, which causes the gas in a wider range of reservoirs to be unable to flow.

Conclusions

In this paper, we tested the DTPG values on cores with different permeability at different stresses and saturations of mobile water. The quantitative relationship between permeability and the DTPG sensitivity coefficients was studied. The threshold pressure distributions of different permeability distribution modes of tight gas reservoirs were calculated based on our experimental data, and the gas production loss of DTPG and FTPG were compared. We obtained the following conclusions based on our experiments:

(1) The DTPG of tight gas reservoir rocks increases logarithmically by 0.5-3.9 times in the effective stress range of 0.6-30.5 MPa, such that rocks with smaller permeability exhibit a stronger stress sensitivity of DTPG.

(2) The DTPG of tight gas reservoir rocks increases exponentially by 2.7-6.5 times from irreducible water saturation to a mobile water saturation of 25%. Once again, rocks with smaller permeability exhibited a stronger mobile water saturation sensitivity of DTPG.

(3) The distribution of increasing permeability in the displacement direction is beneficial to the reduction of the threshold pressure. The influence of the reservoir permeability heterogeneity on the DTPG is smaller at higher pressure.

(4) DTPG causes a 34-45% higher gas production loss in tight reservoirs than FTPG. The distribution of decreasing permeability in the displacement direction makes a 6-8% larger gas production loss than that of an opposite permeability distribution.

Overall, the sensitivity of DTPG to stress and mobile water shows decreasing trends with rock permeability. The threshold pressure is small when the direction of gas flow is consistent with the direction of increasing permeability in heterogeneous reservoirs. Production wells should be located in high permeability sections of heterogeneous reservoirs to reduce the threshold pressure.

List of main abbreviations

TPG	Threshold pressure gradient
DTPG	Dynamic threshold pressure gradient
DTPG	Fixed threshold pressure gradient
DTP	Dynamic threshold pressure
FTP	Fixed threshold pressure
$DTPG_{min}$	DTPG value at minimum effective stress of rock
$DTPG_{max}$	DTPG value at maximum effective stress of rock
P_{eff}	Rock effective stresses
λ	Stress sensitivity coefficient of threshold pressure gradient
η	Mobile water sensitivity coefficient of threshold pressure gradient
S_{wi}	Irreducible water saturation
k	Core permeability
S_m	Mobile water saturation
P_o	Overburden pressure
P_0	Pressure at production end
P_e	Pressure at reservoir edge
K_1	A decreasing permeability distribution mode along the flow direction
K_2	An increasing permeability distribution mode along the flow direction
L	Distance from the production well
P_{emin}	A minimum P_e value, which is just large enough for the gas to start flowing
P_w	Bottom hole flowing pressure
L_p	Gas production loss
ΔL_p	Difference in production loss between dynamic and fixed threshold pressure gradient

Acknowledgments

This research is supported by National Natural Science Foundation of China, “The formation mechanism of residual gas and liquid in coal seam and the geological constraints for effective production” (41872171), and “Cross-scale precipitation mode of asphaltene in ultra-deep sandstone reservoir during CO_2 flooding” (52104048).

References

[1] Wei, J and Wang, K., 2018. A preliminary study of the present-day in-situ stress state in the Ahe tight gas reservoir, Dibei Gasfield, Kuqa Depression. *Marine and Petroleum Geology* 96: 154-165.

[2] Oluwadebi, A. G., Taylor, K.G and Ma, L., 2019. A case study on 3D characterisation of pore structure in a tight sandstone gas reservoir: the Collyhurst Sandstone, East Irish Sea Basin, northern England. *Journal of Natural Gas Science and Engineering* 68: 102917.

[3] Huang, H., Babadagli, T., Chen, X., Li, H., & Zhang, Y., 2020. Performance comparison of novel chemical agents for mitigating water-blocking problem in tight gas sandstones. *SPE Reservoir Evaluation & Engineering* 23.04: 1150-1158.

[4] Nazari, M. H., Tavakoli, V., Rahimpour-Bonab, H., & Sharifi-Yazdi, M., 2019. Investigation of factors influencing geological heterogeneity in tight gas carbonates, Permian reservoir of the Persian Gulf. *Journal of Petroleum Science and Engineering*, *183*, 106341.

[5] Nelson, P. H., 2009. Pore-throat sizes in sandstones, tight sandstones, and shales. *AAPG bulletin*, 93(3), 329-340.

[6] Hu, H., Zeng, Z., & Liu, J., 2015. Key elements controlling oil accumulation within the tight sandstones. *Journal of Earth Science*, 26(3), 328-342.

[7] Wang, J., Wu, S., Li, Q., Zhang, J., & Guo, Q., 2020. Characterization of the pore-throat size of tight oil reservoirs and its control on reservoir physical properties: A case study of the Triassic tight sandstone of the sediment gravity flow in the Ordos Basin, China. *Journal of Petroleum Science and Engineerin*g, 186, 106701.

[8] Zafar, A., Su, Y. L., Li, L., Fu, J. G., Mehmood, A., Ouyang, W. P., & Zhang, M., 2020. Tight gas production model considering TPG as a function of pore pressure, permeability and water saturation. *Petroleum Science*, 17(5), 1356-1369.

[9] Zhao, F., Liu, P., Hao, S., Qiu, X., Shan, C., & Zhou, Y., 2021. A new dynamic capillary-number-recovery evaluation method for tight gas reservoirs. *Journal of Petroleum Science and Engineering*, 204, 108730.

[10] Zeng, J., Wang, X., Guo, J., Zeng, F., & Zhang, Q., 2018. Composite linear flow model for multi-fractured horizontal wells in tight sand reservoirs with the threshold pressure gradient. *Journal of Petroleum Science and Engineering*, 165, 890-912.

[11] Tian, W., Li, A., Ren, X., & Josephine, Y., 2018. The threshold pressure gradient effect in the tight sandstone gas reservoirs with high water saturation. *Fuel*, *226*, 221-229.

[12] Song, H., Cao, Y., Yu, M., Wang, Y., Killough, J. E., & Leung, J., 2015. Impact of permeability heterogeneity on production characteristics in water-bearing tight gas reservoirs with threshold pressure gradient. *Journal of Natural Gas Science and Engineering*, *22*, 172-181.

[13] Wang, Q., Yang, S., Glover, P. W., Lorinczi, P., Qian, K., & Wang, L., 2020. Effect of pore-throat microstructures on formation damage during miscible CO_2 flooding of tight sandstone reservoirs. *Energy & Fuels*, 34(4), 4338-4352.

[14] Wang, Q., Wang, L., Glover, P. W., & Lorinczi, P., 2020. Effect of a Pore Throat Microstructure on Miscible CO_2 Soaking Alternating Gas Flooding of Tight Sandstone Reservoirs. *Energy & Fuels*, 34(8), 9450-9462.

[15] Zafar, A., Su, Y. L., Li, L., Fu, J. G., Mehmood, A., Ouyang, W. P., & Zhang, M., 2020. Tight gas production model considering TPG as a function of pore fluid pressure, permeability and water saturation. *Petroleum Science*, *17*(5), 1356-1369.

[16] Warpinski, N. R., & Teufel, L. W., 1992. Determination of the effective-stress law for permeability and deformation in low-permeability rocks. *SPE Formation Evaluation*, 7(02), 123-131.

[17] Zhu, W., Song, H., Huang, X., Liu, X., He, D., & Ran, Q., 2011. Pressure characteristics and effective deployment in a water-bearing tight gas reservoir with low-velocity non-Darcy flow. *Energy & Fuels*, *25*(3), 1111-1117.

[18] Ding, J., Yang, S., Nie, X., & Wang, Z., 2014. Dynamic threshold pressure gradient in tight gas reservoir. *Journal of Natural Gas Science and Engineering*, *20*, 155-160.

[19] Liu, K., Yin, D. and Su, H., 2020. Transient transfer shape factor for fractured tight reservoirs: Effect of the dynamic threshold pressure gradient in unsteady flow. *Energy Science & Engineering*, 8(7), pp. 2566-2586.

[20] Liu, K., Yin, D., Sun, Y. and Xia, L., 2020. Analytical and experimental study of stress sensitivity effect on matrix/fracture transfer in fractured tight reservoir. *Journal of Petroleum Science and Engineering*, 195, p. 107958.

[21] Wang, X. and Sheng, J.J., 2017. Discussion of liquid threshold pressure gradient. *Petroleum*, 3(2), pp. 232-236.

[22] Wang, Q., Zhu, B., Shen, J., Glover, P. W., Lorinczi, P., & Han, H., 2022. Quantifying Controls on Threshold Pressure during CO_2 Injection in Tight Gas Reservoir Rocks. *Energy & Fuels*.

[23] Cao, L. N., Li, X. P., Luo, C., Yuan, L., Zhang, J. Q., & Tan, X. H., 2016. Horizontal well transient rate decline analysis in low permeability gas reservoirs employing an orthogonal transformation method. *Journal of Natural Gas Science and Engineering*, *33*, 703-716.

[24] Bo, N., Zuping, X., Xianshan, L., Zhijun, L., Zhonghua, C., Bocai, J., & Xiaolong, C.,2020. Production prediction method of horizontal wells in tight gas reservoirs considering threshold pressure gradient and stress sensitivity. *Journal of Petroleum Science and Engineering*, *187*, 106750.

[25] Song, H., Liu, Q., Yang, D., Yu, M., Lou, Y., & Zhu, W.,2014. Production equation of fractured horizontal well in a water-bearing tight gas reservoir with low-velocity non-Darcy flow. *Journal of Natural Gas Science and Engineering*, *18*, 467-473.

[26] Glover, P.W.J. and Luo, M., 2020. The Porosity and Permeability of Binary Grain Mixtures. Transport in Porous Media, 132(1), pp. 1-37.

[27] Walker, E. and Glover, P.W.J., 2010. Permeability models of porous media: Characteristic length scales, scaling constants and time-dependent electrokinetic coupling. *Geophysics*, 75(6), pp. E235-E246.

[28] Glover, P.W.J. and Walker, E., 2009. Grain-size to effective pore-size transformation derived from electrokinetic theory. *Geophysics*, 74(1), pp. E17-E29.

[29] Garum, M., Glover, P.W.J., Lorinczi, P., Scott, G. and Hassanpour, A., 2021. Ultrahigh-Resolution 3D Imaging for Quantifying the Pore Nanostructure of Shale and Predicting Gas Transport. *Energy and Fuels*, 35(1), pp. 702-717.

[30] Garum, M., Glover, P.W.J., Lorinczi, P., Micklethwaite, S. and Hassanpour, A., 2021. Integration of Multiscale Imaging of Nanoscale Pore Microstructures in Gas Shales. *Energy and Fuels*, 35(13), pp. 10721-10732.

[31] Ding, J., Yang, S., Cao, T., & Wu, J., 2018. Dynamic threshold pressure gradient in tight gas reservoir and its influence on well production. *Arabian Journal of Geosciences*, *11*(24), 1-6.

[32] Fu, J., Su, Y., Li, L., Wang, W., Wang, C., & Li, D., 2022. Production model with mechanisms of multiple seepage in tight gas reservoir. *Journal of Petroleum Science and Engineering*, *209*, 109825.

[33] Wu, Z., Cui, C., Lv, G., Bing, S., & Cao, G., 2019. A multi-linear transient pressure model for multistage fractured horizontal well in tight oil reservoirs with considering threshold pressure gradient and stress

sensitivity. *Journal of Petroleum Science and Engineering*, *172*, 839-854.

[34] Lu, C., Qin, X., Ma, C., Yu, L., Geng, L., Bian, H., & Zhou, Y., 2022. Investigation of the impact of threshold pressure gradient on gas production from hydrate deposits. *Fuel*, *319*, 123569.

[35] Liu, G., Xie, S., Tian, W., Wang, J., Li, S., Wang, Y., & Yang, D., 2022. Effect of pore-throat structure on gas-water seepage behaviour in a tight sandstone gas reservoir. *Fuel*, *310*, 121901.

[36] Wang, C., Cheng, Y., Yi, M., Jiang, J., & Wang, D., 2021. Threshold pressure gradient for helium seepage in coal and its application to equivalent seepage channel characterization. *Journal of Natural Gas Science and Engineering*, *96*, 104231.

[37] Liu, B., Yang, Y., Li, J., Chi, Y., Li, J., & Fu, X., 2020. Stress sensitivity of tight reservoirs and its effect on oil saturation: A case study of Lower Cretaceous tight clastic reservoirs in the Hailar Basin, Northeast China. *Journal of Petroleum Science and Engineering*, *184*, 106484.

[38] Zeng, J., Wang, X., Guo, J., & Zeng, F., 2016, August. Analytical model for multi-fractured horizontal wells in tight sand reservoir with threshold pressure gradient. In *SPE Asia Pacific Hydraulic Fracturing Conference*. OnePetro.

[39] Dou, X., Liao, X., Zhao, X., Wang, H., & Lv, S., 2015. Quantification of permeability stress-sensitivity in tight gas reservoir based on straight-line analysis. *Journal of Natural Gas Science and Engineering*, *22*, 598-608.

[40] Liu, G., Yin, H., Lan, Y., Fei, S., & Yang, D., 2020. Experimental determination of dynamic pore-throat structure characteristics in a tight gas sandstone formation with consideration of effective stress. *Marine and Petroleum Geology*, *113*, 104170.

[41] Liu, G., Wang, Y., Yin, H., Ding, Y., Lan, Y., & Yang, D., 2022. Determination of gas-water seepage characteristics with consideration of dynamic pore-throat structure in a tight sandstone gas formation. *Marine and Petroleum Geology*, *136*, 105440.

[42] Shi, H., Lai, F., Shi, G., Liang, Y., & Dai, Y., 2021. Dynamic prediction and influencing factors analysis of gas and water co-production stage in tight sandstone reservoir. *Journal of Natural Gas Science and Engineering*, *96*, 104327.

[43] Zeng, J., Zhang, Y., Zhang, S., Qiao, J., Feng, X., & Feng, S., 2016. Experimental and theoretical characterization of the natural gas migration and accumulation mechanism in low-permeability (tight) sandstone cores. *Journal of Natural Gas Science and Engineering*, *33*, 1308-1315.

[44] Yang, X., Meng, Y., Shi, X., & Li, G., 2017. Influence of porosity and permeability heterogeneity on liquid invasion in tight gas reservoirs. *Journal of Natural Gas Science and Engineering*, *37*, 169-177.

[45] Qu, Y., Sun, W., Tao, R., Luo, B., Chen, L., & Ren, D., 2020. Pore–throat structure and fractal characteristics of tight sandstones in Yanchang Formation, Ordos Basin. *Marine and Petroleum Geology*, *120*, 104573.

[46] Cheng, Y., Zhang, C., & Zhu, L. Q., 2017. A fractal irreducible water saturation model for capillary tubes and its application in tight gas reservoir. *Journal of Petroleum Science and Engineering*, *159*, 731-739.

[47] Dong, M., Shi, X., Ling, S., Zhang, B., & Li, X., 2019. Effect of dynamic pseudo threshold pressure gradient on well production performance in low-permeability and tight oil reservoirs. *Journal of Petroleum Science and Engineering*, *173*, 69-76.

[48] Al-Zainaldin, S., Glover, P.W.J. and Lorinczi, P., 2017. Synthetic Fractal Modelling of Heterogeneous and Anisotropic Reservoirs for Use in Simulation Studies: Implications on Their Hydrocarbon Recovery Prediction. *Transport in Porous Media*, 116(1), pp. 181-212.

[49] Glover, P.W.J., Lorinczi, P., Al-Zainaldin, S., Al-Ramadhan, H., Sinan, S. and Daniel, G., 2019. A fractal approach to the modelling and simulation of heterogeneous and anisotropic reservoirs, *Society of Petroleum Engineers* - SPE Offshore Europe Conference and Exhibition 2019, OE 2019.

[50] Glover, P.W.J., Lorinczi, P., Al-Zainaldin, S., Al-Ramadan, H., Daniel, G. and SINAN, S., 2018. Advanced fractal modelling of heterogeneous and anisotropic reservoirs, *SPWLA 59th Annual Logging Symposium* 2018.

[51] Sinan, S., Glover, P.W.J. and Lorinczi, P., 2020. Modelling the Impact of Anisotropy on Hydrocarbon Production in Heterogeneous Reservoirs. *Transport in Porous Media*, 133(3), pp. 413-436.

[52] Diwu, P., Liu, T., You, Z., Jiang, B., & Zhou, J., 2018. Effect of low velocity non-Darcy flow on pressure response in shale and tight oil reservoirs. *Fuel*, *216*, 398-406.